ADVANCED FUNCTIONAL MATERIALS
www.afm-journal.de

The Metallic Nature of Epitaxial Silicene Monolayers on Ag(111)

Neil W. Johnson, Patrick Vogt, Andrea Resta, Paola De Padova, Israel Perez, David Muir, Ernst Z. Kurmaev, Guy Le Lay, and Alexander Moewes*

Silicene is a two-dimensional structure composed of a buckled hexagonal honeycomb lattice of silicon atoms. Freestanding silicene is yet to be synthesized, but epitaxial silicene monolayers have been directly observed or predicted to exist on a number of supporting substrates. Herein the atomic and electronic structures of five distinct epitaxial silicene morphologies on Ag(111) are examined through the complementary techniques of density functional theory and soft X-ray spectroscopy at the Si $L_{2,3}$ edge. Hybridization with the Ag(111) substrate is shown to cause these silicene monolayers to become strongly metallic, and the specific electronic interactions that are responsible for this metallic nature are determined. The results imply that epitaxial silicene on Ag(111) does not possess the Dirac cone electronic structure that is characteristic of freestanding silicene and graphene sheets.

1. Introduction

Early theoretical investigations into a silicon-based analogue to graphene, including tight-binding models[1] and density functional theory (DFT) calculations,[2] supported the idea that freestanding silicene monolayers possess the same zero-bandgap Dirac cone electronic structure that is responsible for graphene's intriguing electronic and magnetic characteristics.[3] However, freestanding silicene has not yet been isolated in the laboratory largely due to the lack of a naturally occurring silicon-based analogue to graphite. Silicene is an attractive alternative to graphene as semiconductor device manufacturers are already well-equipped to deal with silicon-based components, whereas the transition to carbon-based electronics could present significant challenges in device manufacturing and design. Further, the buckling inherent in silicene could allow for the tuning of its bandgap and polarized spin-states in the presence of an external electric field,[4,5] making it a good candidate material for spintronic applications. Freestanding silicene is also predicted to be a two-dimensional topological insulator due to quantum spin Hall effects.[6,7] An excellent review of this novel material has recently been published.[8]

While it is possible to chemically exfoliate thin sheets of Si, and possibly even Si monolayers, from $CaSi_2$,[9] most reports of silicene monolayers have involved physical deposition of Si on a supporting substrate. Typically the substrate used is Ag(111)[10–12] (the focus of this investigation), but stable monolayers have also been reported on Ir(111)[13] and ZrB_2(0001),[14] and simulations have suggested it may also be possible to deposit a silicene monolayer on h-BN.[15,16] However, the atomic and electronic structures of these epitaxial silicene sheets can deviate significantly from those of freestanding silicene due to electronic interaction with the substrate, in contrast to graphene which has been shown to be minimally perturbed by an underlying Ag(111) substrate.[17] Understanding the nature of this interaction and knowing its effects on the electronic properties of the epitaxial silicene monolayer will be an important step toward the realization of the potential applications for this novel material.

Scanning tunneling microscopy (STM) and DFT investigations of epitaxial silicene on Ag(111) suggest that it is capable of taking on a number of stable forms, depending on the deposition rate and substrate temperature during growth.[11,18–20] The first report of epitaxial silicene depicted a monolayer (3×3) Si reconstruction on a (4×4) Ag(111) supercell.[10] Angle-resolved photoemission spectroscopy (ARPES) measurements were initially thought to indicate the presence of a Dirac cone with a bandgap opening,[10] but a subsequent DFT bandstructure calculation suggested that the observed linear band was the

N. W. Johnson, Dr. I. Perez,
Dr. D. Muir,[+] Prof. A. Moewes
University of Saskatchewan
116 Science Place, Saskatoon S7N 5E2, Canada
E-mail: johnson.neil@usask.ca
Dr. P. Vogt
Technische Universität Berlin
Hardenbergstrasse 36, Berlin 10623, Germany
Dr. A. Resta,[++] Prof. G. Le Lay
Aix-Marseille University PIIM-CNRS
Campus de Saint Jérôme
Marseille Cedex 20, France
Dr. P. De Padova
Consiglio Nazionale delle Ricerche-ISM
via Fosso del Cavaliere, Rome 00133, Italy
Prof. E. Z. Kurmaev
Institute of Metal Physics
Russian Academy of Sciences – Ural Division
Yekaterinburg GSP-170, 620219, Russia

[+]Present address: Canadian Light Source, 44 Innovation Boulevard, Saskatoon S7N 5B3, Canada
[++]Present address: SOLEIL Synchrotron, L'Orme des Merisiers, Saint-Aubin, F-91190, France

DOI: 10.1002/adfm.201400769

product of Si hybridization with Ag states,[21] not an arm of silicene's Dirac cone. Presently, it remains controversial whether silicene on Ag(111) is inherently metallic[21–24] or a semiconductor with a small gap,[25,26] though the majority of publications seem to support the former conclusion.

A number of other stable silicene morphologies on Ag(111) have since been observed or predicted, including silicene reconstructions on $(2\sqrt{3} \times 2\sqrt{3})R30°$,[18] $(\sqrt{7} \times \sqrt{7})R19.1°$,[18] and $(\sqrt{13} \times \sqrt{13})R13.9°$[11,18,27–30] Ag(111). In this study, we use the complementary techniques of DFT calculations and synchrotron-based soft X-ray spectroscopy to explore the electronic structures of monolayer silicene reconstructions on (4×4) and $(\sqrt{13} \times \sqrt{13})R13.9°$ Ag(111), the two most commonly observed reconstructions in the literature. We report that ab initio DFT calculations predict a metallic electronic structure for both of these epitaxial monolayers; a prediction which we support by experimentally probing the valence and conduction bands with soft X-ray absorption and non-resonant emission spectroscopy (XAS and XES).

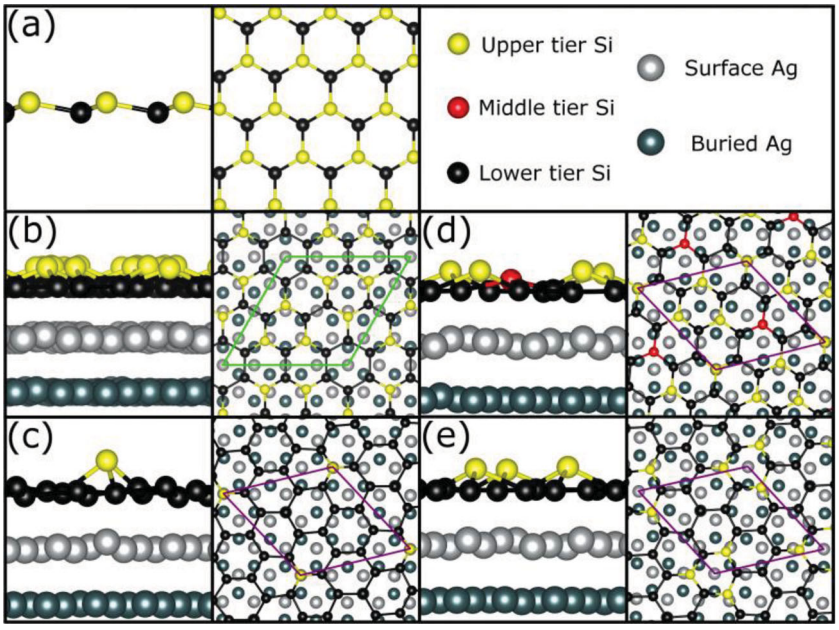

Figure 1. a) The structure of low-buckled freestanding silicene. Note the sublattice inversion symmetry of the upper and lower layers. The relaxed structures of b) $(3 \times 3)/(4 \times 4)$ and c-e) $(\sqrt{7} \times \sqrt{7})/(\sqrt{13} \times \sqrt{13})$ epitaxial silicene. $(3 \times 3)/(4 \times 4)$ silicene has 18 Si atoms per unit cell for a coverage ratio of 1.125 Si:Ag, while the $(\sqrt{7} \times \sqrt{7})/(\sqrt{13} \times \sqrt{13})$ silicene structures contain 14 Si sites per unit cell for a coverage ratio of 1.077 Si:Ag. Visualization provided by the VESTA software package.[34]

2. Density Functional Theory Calculations

DFT refinements of the atomic structures and calculation of the electronic structures of epitaxial silicene sheets were performed with the WIEN2k software package,[31] which is based on the full-potential linearized augmented plane wave + local orbitals method. The epitaxial silicene was modelled as sheets of Si covering both faces of a five unit cell thick slab of Ag(111) in the Pm (No. 6) space group. This space group is symmetric about the plane z = 0.5 where **z** is in the direction perpendicular to the Ag(111) surface. 15 Å of vacuum in the **z** direction separated each silicene sheet in order to isolate adjacent slabs from each other. All calculations were performed on a $(10 \times 10 \times 1)$ k-point mesh with a –6.0 Ry plane-wave cutoff energy and an RKMAX of 5.0. Calculations were considered to have converged when energy and charge steps in self-consistent field iterations dropped below 10^{-4} Ry and 10^{-3} e, respectively. The internal positions of atoms were optimized such that the net force on each atom fell below 1 mRy/a.u. Both structural relaxations and electronic structure calculations used the generalized gradient approximation of Perdew, Burke, and Ernzerhof[32] (PBE-GGA). Calculations using the modified Becke-Johnson exchange-correlation functional were also performed, as these usually provide better estimates of the bandgap,[33] but the results were found to be virtually identical to the PBE-GGA calculations in terms of the DOS in the vicinity of the Fermi level.

We first perform DFT optimizations and electronic structure calculations on freestanding silicene as a test of the validity of our theoretical approach. An optimization of the buckling distance and Si–Si bond length is found to reproduce the structural parameters of low-buckled (LB) silicene reported in Reference [2]. This relaxed structure is shown in **Figure 1**a.

Our internal force minimization of the epitaxial silicene sheets uses the published structures of (3×3) silicene on a coincident (4×4) Ag(111) supercell,[10] three unique configurations of $(\sqrt{7} \times \sqrt{7})R19.1°$ silicene on a coincident $(\sqrt{13} \times \sqrt{13})R13.9°$ Ag(111) supercell[18,20,29,35] (hereafter $(\sqrt{7} \times \sqrt{7})/(\sqrt{13} \times \sqrt{13})$), and (3×3) silicene on a coincident $(\sqrt{13} \times \sqrt{13})R13.9°$ Ag(111) supercell[11] (hereafter $(3 \times 3)/(\sqrt{13} \times \sqrt{13})$) as initial configurations. We find most of these structures to be nearly optimal already, with the exception of $(3 \times 3)/(\sqrt{13} \times \sqrt{13})$, which we observe to deviate significantly from the simple buckled structure reported previously,[11] resulting in a relaxed structure that can no longer be said to contain a hexagonal honeycomb of Si atoms on the surface. By explicitly imposing hexagonal symmetry, the Si surface structure is found to relax to a distorted, highly buckled honeycomb closely resembling the simulated STM image,[11] but this configuration is unstable when the symmetry constraints are subsequently removed. As such, we do not consider this particular configuration any further in this study, and suggest that it is not likely to be physically realized. The optimized structures of $(3 \times 3)/(4 \times 4)$ and the three forms of $(\sqrt{7} \times \sqrt{7})/(\sqrt{13} \times \sqrt{13})$ silicene are described in Figure 1b–e.

With the freestanding and epitaxial silicene structures optimized, the ground-state density of states (DOS) for each can be explored in detail. **Figure 2**a shows the calculated partial and total Si DOS for freestanding silicene, which are in good agreement with previous DFT and tight-binding model calculations.[2] The lowest-lying states in the valence band are predominantly Si *s* states, which give way to Si *sp* hybrid states in the range of –8 to

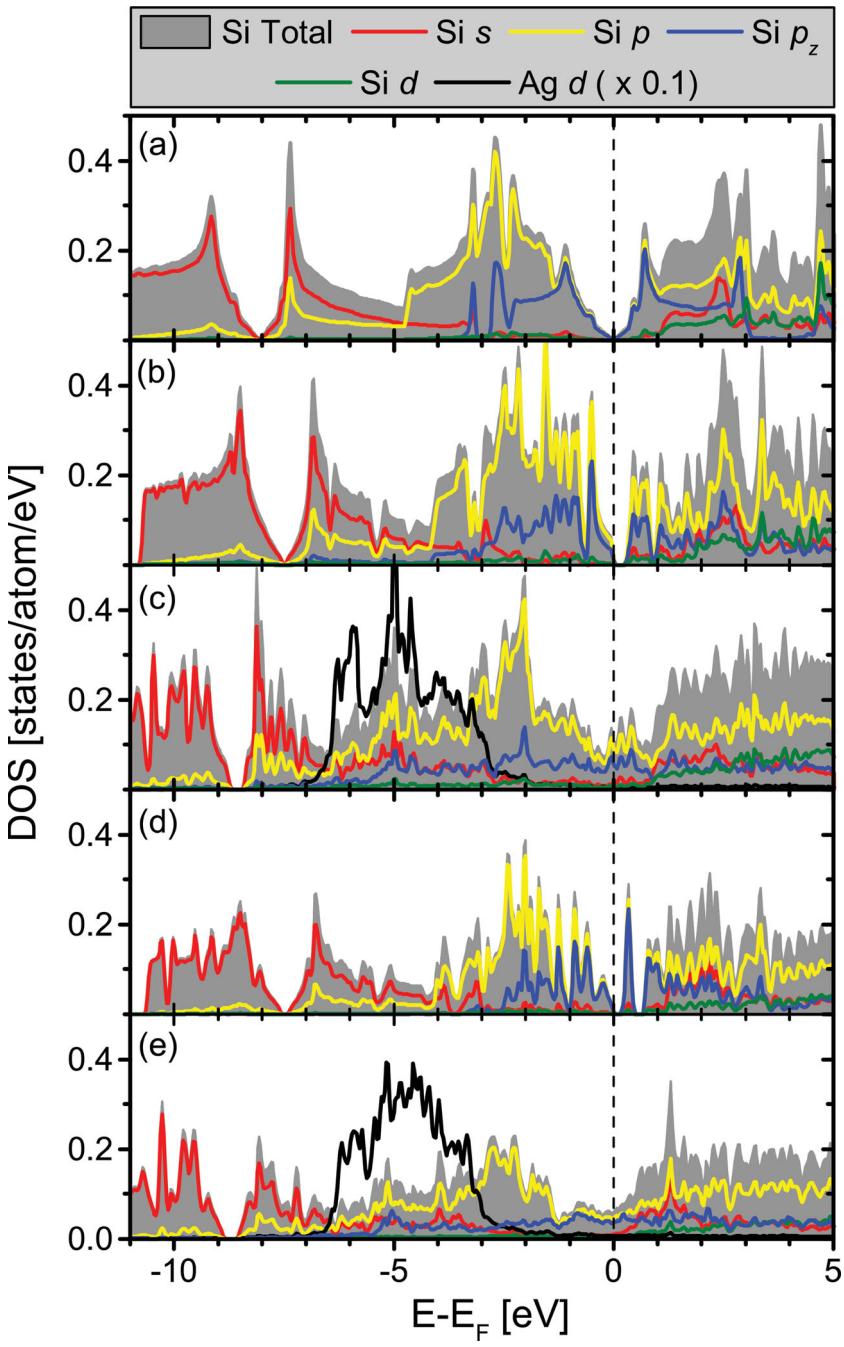

Figure 2. a) The calculated DOS of freestanding silicene, exhibiting a zero-bandgap electronic structure. b,d) The calculated DOS of (3×3)/(4×4) and (√7× √7)/(√13× √13) silicene (respectively) in the absence of a supporting Ag(111) substrate. In this case, symmetry-breaking causes the degeneration of the Dirac cone, opening up a small bandgap. c,e) The calculated DOS of (3 × 3)/(4 × 4) and (√7 × √7)/(√13 × √13) silicene (respectively) including the Ag(111) substrate. In these structures, hybridization with the Ag *d* states and the presence of the Ag *sp* band cause the Si p_z states to span the Fermi level, resulting in metallic silicene.

–3 eV (Si–Si σ bonding). The top of the valence band and bottom of the conduction band are composed primarily of p_z states, akin to the π bonding states observed in graphene. The DOS exhibits a similar zero-bandgap electronic structure, the result of occupied and unoccupied Si p_z bands that have a linear dispersion relation in the vicinity of the Fermi energy. It is worth mentioning that this is only true for calculations that use a single k-point in the direction perpendicular to the silicene plane, as including more k-points in this direction forces interaction between adjacent sheets and moves the band crossing away from the Fermi level.

We perform similar electronic structure calculations on the epitaxial silicene sheets, both with and without the underlying Ag(111) slab (Figure 2b–e). As the electronic structures of the three types of (√7 × √7)/(√13 × √13) silicene are found to be virtually indistinguishable, only the results of calculations derived from the silicene structure in Figure 1c will be displayed and discussed.

The bandstructure of silicene in the (3 × 3)/(4 × 4) configuration in the absence of a supporting Ag(111) slab has already been reported in the literature.[36] We confirm these theoretical results, observing that the DOS is largely unchanged from that of LB silicene, save for the opening of a 0.3 eV bandgap owing to the sublattice symmetry-breaking causing the degeneration of the Dirac cone (Figure 2b). When extending the same treatment to (√7 × √7)/(√13 × √13)-type silicene structures, we also report the opening of a 0.2 eV bandgap in these materials in the absence of a supporting substrate (Figure 2d). In the (3 × 3)/(4 × 4) case, we see the Si p_z states leaking further down into the valence band, suggesting a more sp^3-like hybridization scheme than in the freestanding silicene. This is not apparent in the (√7 × √7)/(√13 × √13) case, which is expected because the coverage factor is lower for these sheets, resulting in a more planar configuration.

However, when the Ag slab is included in the DFT calculations, the results are markedly different. For (3 × 3)/(4 × 4) silicene (Figure 2c) as well as each of the (√7 × √7)/(√13 × √13) silicene structures (Figure 2e), the resulting DOS is strongly metallic, with a continuation of Si p_z states across the Fermi level. These p_z states are almost uniformly spread across the DOS from the bottom of the Ag *d* states upwards, exhibiting strong hybridization with the Si *s* and Ag *d* states at about 5 eV below the Fermi level. This indicates that the p_z states are playing a large role in σ bonding, which is indicative of the sp^3 hybridization scheme. As a result, the π-like bonds in these epitaxial silicene monolayers deteriorate and their constituent p_z states bend downward across the Fermi level. Our interpretation is that the strong hybridization between Si *p* and Ag *d* states significantly perturbs the electronic structure of the silicene sheet, and the availability of the Ag *sp* states for hybridization allows for the

Si *p* states to populate what would normally be the gap region of the isolated silicene sheet. This rehybridization scenario can be contrasted against the rigid band model that describes alkali-metal-doped Si clathrates,[37] in which the introduction of a metallic donor species simply shifts the Fermi energy without significantly affecting the bandstructure of the material.

The WIEN2k utility XSPEC is used to estimate ground-state Si $L_{2,3}$ emission spectra from the occupied DOS and absorption spectra from the unoccupied DOS[38] (**Figure 3**a), for comparison to their corresponding soft X-ray measurements. Because the final state of an X-ray absorption process contains a core-hole (a Si 2*p* core-hole in our case), we do not expect the ground state absorption spectra to agree completely with our XAS measurements as the core-hole tends to enhance features at the bottom of the conduction band and occasionally shifts the bottom of the conduction band downward in energy, reducing the apparent band gap of the material. To account for this effect we also perform DFT calculations with a Si 2*p* core-hole present in each of the unique Si sites within each of the epitaxial silicene structures, which are averaged together for each material to produce the core-hole absorption spectra represented by dashed lines in Figure 3.

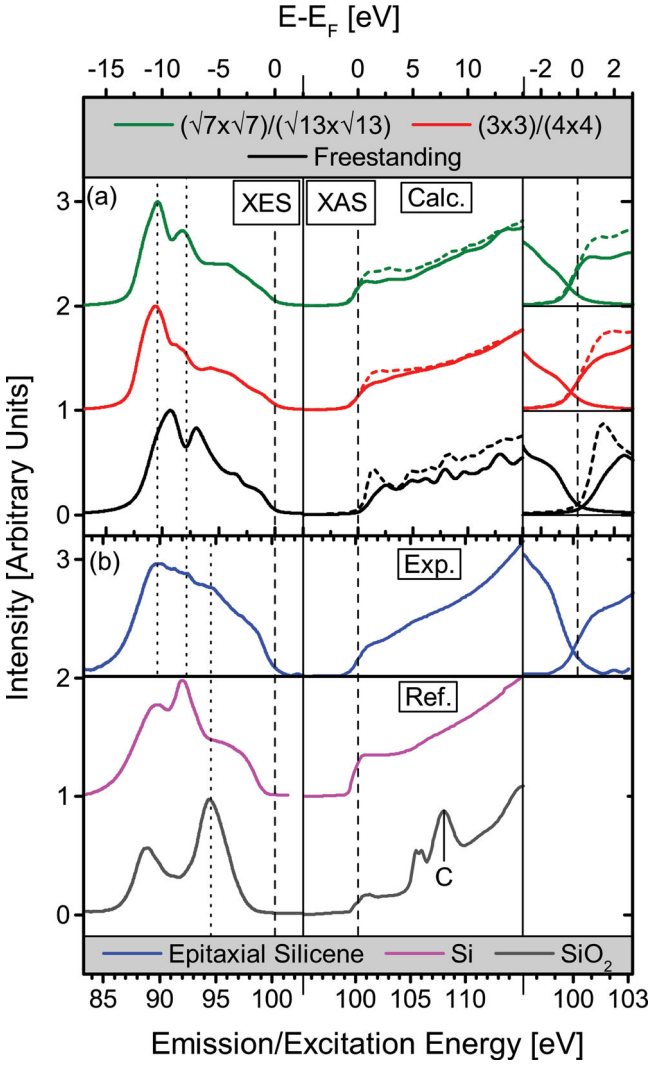

Figure 3. a) Theoretical XES and XAS spectra obtained from the calculated Si pDOS for epitaxial and freestanding silicene. The Fermi energy is marked by a dashed vertical line. Calculated XAS spectra including a Si 2*p* core-hole are indicated by a dashed line. b) XES and XAS measurements of epitaxial silicene and Si references (a sputtered crystalline Si wafer in fuchsia and an amorphous SiO_2 crystal (XES) and native SiO_2 oxide on a Si wafer (XAS) in black). Dotted lines indicate peaks in the XES spectrum and the calculated or measured features they are attributed to. The overlaps of the measured and calculated XES and XAS spectra, which are used as a metric for the degree to which the substances are metallic, are shown in the rightmost panels, magnified 2× vertically and on an enlarged horizontal range.

As Si $L_{2,3}$ absorption and emission spectra are related to transitions to and from the Si 2*p* core level, we expect them to predominantly resemble the *s* and *d* character in the conduction and valence bands due to the dipole selection rule for electronic transitions. Indeed, the two most prominent features in the calculated emission spectrum of freestanding silicene are due to the low-lying *s* states at 7 and 10 eV below the Fermi energy, including the ones in the σ bonding region near the middle of the valence band (Figure 3a). The intensity drops off near the high end of the valence band, because this energy region is dominated by Si *p* states. The calculated ground-state Si 2*p* XAS spectrum has a gradual onset, with the lowest energy peak a couple of eV above the Fermi level owing to the Si *s* and *d* states concentrated near the bottom of the conduction band. Features further up the absorption spectrum are the result of the sharp peaks in the conduction band DOS, largely composed of Si *d* character. When one full Si 2*p* core-hole is included in a (5 × 5 × 1) supercell (to prevent the overestimation of core-hole effects due to core-hole/core-hole interaction), the onset becomes sharper due to the enhancement of states at the bottom of the conduction band, but does not seem to shift downward in energy appreciably. The small overlap of the calculated XAS and XES in the vicinity of the Fermi level is due to the 0.6 eV spin-orbit splitting of the $L_{2,3}$ core levels and the intentional broadening applied to the transition-weighted partial density of states (pDOS) to simulate the instrumental broadening that occurs in the actual measurements.

Similar calculations of the Si $L_{2,3}$ XES and Si 2*p* XAS spectra for epitaxial silicene are also shown in Figure 3a. In these spectra, the two major features in the freestanding silicene XES are shifted down in energy in the spectra of the epitaxial sheets, and the valence band width appears to be somewhat larger. The shoulder at the top of the valence band is less pronounced, owing to the broadening of the Si *s* states in this region. The calculated XAS spectra contain far fewer features, as the Si *d* states are relatively smooth in the conduction band, in contrast to those of freestanding silicene. The absorption edge onset also appears to occur at a lower energy, owing to the increased intensity of Si *s* states at the bottom of the conduction band, as well as the weak continuation of *s* and *d* states across the Fermi level. Again, including a core-hole has the effect of enhancing low-lying conduction states without appreciably shifting the nominal absorption onset. Unlike with freestanding silicene, the epitaxial silicene core-hole calculations were not performed on a supercell, because we consider the size of the epitaxial unit cell to be large enough to ensure adequate core-hole separation.

Owing to the encroachment of *s* and *d* states toward the Fermi level, the band overlaps observed in the calculated epitaxial silicene spectra are visibly larger than that of

freestanding silicene. Observing a similar degree of band overlap in soft X-ray spectroscopy measurements of epitaxial silicene would then suggest an experimental confirmation of its predicted metallic nature.

3. Sample Synthesis

Our experiments use a single crystal Ag(111) disk, 8 mm in diameter, as a substrate for silicene growth. The disk is treated with two consecutive cleaning cycles, each consisting of sputtering with 1 kV Ar^+ ions at 10^{-6} Torr for 1 h and annealing at 500 °C for 20 min, in order to remove surface contaminants and ensure a uniform substrate. Si atoms are deposited onto the Ag(111) surface through the resistive heating evaporation of a Si wafer under ultra-high vacuum (UHV, $<5 \times 10^{-9}$ Torr) at a distance of 15 cm from the Ag disk. With our source and sample geometry, a deposition time of 1 h is determined to be sufficient for producing a silicene monolayer, supported by the absence of strong ($\sqrt{3} \times \sqrt{3}$) points with reference to the underlying silicene monolayer on the low energy electron diffraction (LEED) pattern (**Figure 4**) that indicate the presence of a second layer, and remain through the deposition of a multilayer.[28,39–41] A constant substrate temperature of about 270 °C is found to produce a monolayer containing silicene reconstructions on both (4 × 4) and ($\sqrt{13} \times \sqrt{13}$)R13.9° Ag(111). STM topographs of a sample grown under similar conditions show the large domains composed of these distinct morphologies (**Figure 5**). After synthesis, the sample is exposed to a high-vacuum environment ($\approx 2 \times 10^{-7}$ Torr) for approximately 15 min during transport to the soft X-ray spectroscopy chamber, resulting in a net exposure of about 90 langmuir prior to measurement.

4. Soft X-Ray Spectroscopy

We report non-resonant XES and XAS measurements performed on epitaxial silicene monolayers on Ag(111). XES at the Si $L_{2,3}$-edge is used to map the occupied Si *s* and *d* pDOS in the valence band, while Si 2*p* XAS in the surface-sensitive total electron yield (TEY) mode is used to probe the unoccupied Si *s* and *d* pDOS in the conduction band. Si K-edge XES and XAS measurements were attempted in order to probe the occupied and unoccupied Si *p* states in the valence and conduction bands, but the resolution and statistical power of these measurements were found to be inadequate for bandgap determination. In order to obtain an adequate energy resolution at the Si K-edge, the resolving power of the beamline must be ≈18× higher than it would be for the same resolution at the $L_{2,3}$-edge. While this is achievable, it inevitably reduces the statistical power of the measurements. Another issue arises from the increased penetration depth of the Si K-edge photons, which results in less overall signal coming from the epitaxial Si monolayer.

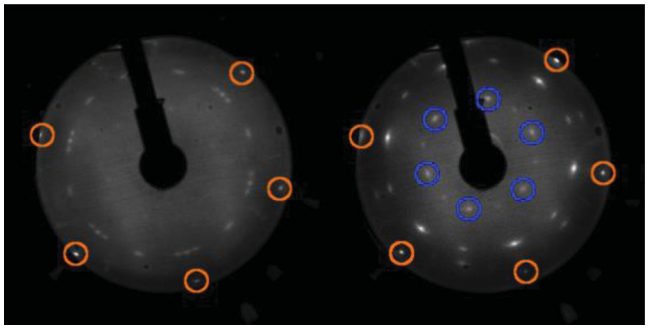

Figure 4. 59 eV LEED patterns for our epitaxial silicene monolayer (left, 1 h deposition) and a thin multilayer (right, 2 h deposition) grown on Ag(111). Orange circles indicate the underlying Ag(111) points, and blue circles indicate points resulting from the reconstruction on the first silicene layer that is typically attributed to the growth of a second layer. The faintness of these points in the LEED pattern of our sample indicates that we deposited very close to a single monolayer. Points originating from (4 × 4) and ($\sqrt{13} \times \sqrt{13}$)R13.9° reconstructions dominate the silicene LEED pattern.

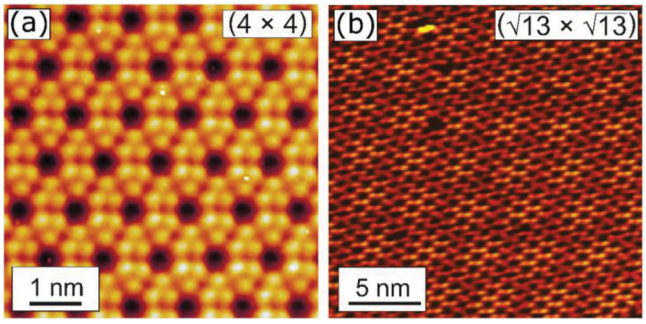

Figure 5. a) High-resolution STM topograph (6 × 6 nm, $U_{bias} = -1.12$ V, I = 0.65 nA) of the (4 × 4) silicene monolayer. Clearly visible is the "flower-like" pattern that results from the upward displacement of 6 of the 18 Si atoms in the honeycomb structure. b) STM topograph (21.6 × 21.6 nm, $U_{bias} = -1.20$ V, I = 1.08 nA) of "($\sqrt{13} \times \sqrt{13}$)" silicene. This "($\sqrt{13} \times \sqrt{13}$)" structure has a clear Moiré-like surface pattern, related to locally well-ordered areas that appear bright in the filled-states STM image which are surrounded by less-ordered (dark) areas. This means that the long-range order and thus the translational symmetry are disturbed. However, since this structure has a ($\sqrt{13} \times \sqrt{13}$)-like LEED pattern, it is referred to as "(R13 × R13)". STM topographs were obtained under UHV conditions ($<2 \times 10^{-10}$ Torr).

The Si $L_{2,3}$-edge soft X-ray spectroscopy measurements were performed at the XES endstation of the REIXS beamline (10-ID2) at the Canadian Light Source at the University of Saskatchewan. The monochromator resolving power ($E/\Delta E$) was 1×10^4 at the Si $L_{2,3}$-edge energy. The emission spectrometer, which uses diffraction gratings in a Rowland circle geometry as dispersive elements and is fitted with a microchannel plate detector, had a resolving power of ($E/\Delta E$) = 10^3 in the same energy region. Oxygen K-edge X-ray absorption spectra were obtained prior to Si $L_{2,3}$-edge measurements to ensure that the sample had not oxidized significantly during the in vacuo transfer from the preparation chamber to the measurement chamber. The elliptically polarizing undulator was tuned to produce horizontally polarized photons. All reported measurements were performed with an incidence angle of 70° from the normal, and the XES spectrometer collected photons at 90° from the incident beam.

XAS data were calibrated such that the Si–O hybridization feature labelled C in Figure 3 in the TEY absorption spectrum of the native surface oxide on a Si wafer occurred at 108.1 eV. A

series of elastic scattering measurements was used to scale and shift the energy axis of the spectrometer to agree with that of the monochromator, guaranteeing a consistent energy calibration between the XES and XAS.

The measured XES and XAS spectra of our epitaxial sample (composed of $(3 \times 3)/(4 \times 4)$ and $(\sqrt{7} \times \sqrt{7})/(\sqrt{13} \times \sqrt{13})$ silicene) are shown in Figure 3b, alongside those of Si reference materials. As predicted by our DFT calculations, the valence band width is found to be roughly 10 eV in the XES spectrum, and the most prominent feature occurs at the bottom of the valence band, at around 90 eV. There also appears to be a faint feature around 92.5 eV which occurs at the right energy to be a result of the Si σ bonding states. In general, though, the XES spectrum is fairly featureless, which is not unexpected because it is likely the summation of the contributions of two (or more) species of epitaxial silicene.

The weak feature at 95 eV was observed to fluctuate in intensity across the substrate, and slowly increase in intensity with exposure to the incident beam. While it is at approximately the right energy to correspond to Si–Ag *d* hybridization, it also coincides with the main emission feature in the spectrum of SiO_2, which leads us to attribute it to a very mild localized oxidization of the silicene sheet that is exacerbated by beam exposure. The high-energy shoulder near the Fermi level appears to be more pronounced in this measurement than it is predicted to be in any of the epitaxial silicene calculations, suggesting a higher concentration of Si *s* and *d* states at the top of the valence band. This could indicate a stronger hybridization between Si *s* and *p* states (i.e., more sp^3-like) than is predicted in the calculation.

As expected, the XAS is largely featureless and has a smooth onset. We find that it overlaps significantly with the high-energy side of the XES spectrum (shown in the right inset of Figure 3), much more so than what would be expected in a zero-bandgap material like freestanding silicene. It is for this reason, as well as the good general agreement between our calculated and measured soft X-ray spectra, that we suggest that our XES and XAS measurements confirm the DFT-predicted metallic nature of epitaxial silicene on Ag(111).

5. Conclusions

In this work, we use full-potential DFT calculations to relax the predicted atomic structures of silicene reconstructions on (4×4) and $(\sqrt{13} \times \sqrt{13})$R13.9° Ag(111). We find that one of the predicted silicene structures, $(3 \times 3)/(\sqrt{13} \times \sqrt{13})$, is unstable when no symmetry restrictions on the structure are imposed. We therefore rule out the only proposed silicene superstructure on $(\sqrt{13} \times \sqrt{13})$ R13.9° Ag(111) that was not of the $(\sqrt{7} \times \sqrt{7})$R19.1° variety.

We show that full-potential DFT calculations predict that all of the epitaxial silicene monolayers we consider to be metallic in nature. While the substrate-induced sublattice symmetry breaking would normally open up a small bandgap in these structures, strong sp^3-like hybridization between Si atoms and the Ag substrate's *d* states as well as the presence of the Ag *sp* band cause the Si p_z states to span the Fermi level, resulting in metallic epitaxial silicene. The results of these DOS calculations are verified by the excellent agreement between predicted and measured XES and XAS spectra, especially in the overlap region composed of the valence band maximum and conduction band minimum.

Recently, the validity of using LDA and GGA-based calculations for the electronic structures of epitaxial silicene on Ag(111) has been called into question as these techniques ignore the van der Waals (vdW) interaction, which may be quite significant in monolayers supported by metallic substrates. Some authors suggest that the inclusion of vdW forces will have little or no effect on the outcome of electronic structure calculations,[36] while others think it may mean the difference between observing semiconducting and metallic silicene.[25] The excellent correspondence between our calculations and measurements imply that the effect of the vdW interaction is negligible, or at least is not enough to alter the metallic nature of the epitaxial silicene.

This study adds to the growing evidence supporting the conclusion that silicene on Ag(111) is unavoidably metallic due to the strong interaction between Si and Ag, and is therefore not a suitable candidate for exploiting the properties of a 2D material. We suggest that future investigations of monolayer silicene focus on the search for non-metallic substrates which interact more weakly with the epitaxial sheet and allow it to preserve its ideal LB structure. Recent evidence also suggests that silicene multilayers grown on Ag(111) may be a fruitful avenue in the pursuit of two-dimensional silicene.[39–41]

Acknowledgements

The authors gratefully acknowledge financial support from the Natural Sciences and Engineering Research Council of Canada (NSERC) and the Canada Research Chair Program, the "2D-NANOLATTICES" project of the Future and Emerging Technologies (FET) program within the 7th framework program for research of the European Commission under FET Grant No. 270749, the Deutsche Forschungsgemeinschaft (DFG) under Grant No. VO1261/3–1, support from CONACYT Mexico under grant 186142, and the Russian Foundation for Basic Research (Projects 14–02–00006). Calculations utilized Compute Canada's WestGrid HPC consortium. Research was performed at the REIXS beamline of the Canadian Light Source, which is supported by NSERC, the National Research Council (Canada), the Canadian Institutes of Health Research, the Province of Saskatchewan, Western Economic Diversification Canada, and the University of Saskatchewan.

Received: March 8, 2014
Revised: April 3, 2014
Published online: June 10, 2014

[1] G. Guzmán-Verri, L. Lew Yan Voon, *Phys. Rev. B* **2007**, *76*, 075131.
[2] S. Cahangirov, M. Topsakal, E. Aktürk, H. Sahin, S. Ciraci, *Phys. Rev. Lett.* **2009**, *102*, 236804.
[3] A. K. Geim, K. S. Novoselov, *Nat. Mater.* **2007**, *6*, 183.
[4] N. D. Drummond, V. Zólyomi, V. I. Fal'ko, *Phys. Rev. B* **2012**, *85*, 075423.
[5] W.-F. Tsai, C.-Y. Huang, T.-R. Chang, H. Lin, H.-T. Jeng, A. Bansil, *Nat. Commun.* **2013**, *4*, 1500.
[6] C.-C. Liu, W. Feng, Y. Yao, *Phys. Rev. Lett.* **2011**, *107*, 076802.
[7] M. Ezawa, *Eur. Phys. J. B* **2012**, *85*, 363.
[8] Q. Tang, Z. Zhou, *Prog. Mater. Sci.* **2013**, *58*, 1244.
[9] H. Nakano, T. Mitsuoka, M. Harada, K. Horibuchi, H. Nozaki, N. Takahashi, T. Nonaka, Y. Seno, H. Nakamura, *Angew. Chem. Int. Ed.* **2006**, *45*, 6303.

[10] P. Vogt, P. De Padova, C. Quaresima, J. Avila, E. Frantzeskakis, M. Asensio, A. Resta, B. Ealet, G. Le Lay, *Phys. Rev. Lett.* **2012**, *108*, 155501.
[11] C.-L. Lin, R. Arafune, K. Kawahara, N. Tsukahara, E. Minamitani, Y. Kim, N. Takagi, M. Kawai, *Appl. Phys. Express* **2012**, *5*, 045802.
[12] D. Chiappe, C. Grazianetti, G. Tallarida, M. Fanciulli, A. Molle, *Adv. Mater.* **2012**, *24*, 5088.
[13] L. Meng, Y. Wang, L. Zhang, S. Du, R. Wu, L. Li, Y. Zhang, G. Li, H. Zhou, W. A. Hofer, H.-J. Gao, *Nano Lett.* **2013**, *13*, 685.
[14] A. Fleurence, R. Friedlein, T. Ozaki, H. Kawai, Y. Wang, Y. Yamada-Takamura, *Phys. Rev. Lett.* **2012**, *108*, 1.
[15] T. P. Kaloni, M. Tahir, U. Schwingenschlögl, *Sci. Rep.* **2013**, *3*, 3192.
[16] L. Li, X. Wang, X. Zhao, M. Zhao, *Phys. Lett. A* **2013**, *377*, 2628.
[17] B. Kiraly, E. V. Iski, A. J. Mannix, B. L. Fisher, M. C. Hersam, N. P. Guisinger, *Nat. Commun.* **2013**, *4*, 2804.
[18] H. Jamgotchian, Y. Colignon, N. Hamzaoui, B. Ealet, J. Y. Hoarau, B. Aufray, J. P. Bibérian, *J. Phys.: Condens. Matter* **2012**, *24*, 172001.
[19] B. Feng, Z. Ding, S. Meng, Y. Yao, X. He, P. Cheng, L. Chen, K. Wu, *Nano Lett.* **2012**, *12*, 3507.
[20] J. Gao, J. Zhao, *Sci. Rep.* **2012**, *2*, 861.
[21] S. Cahangirov, M. Audiffred, P. Tang, A. Iacomino, W. Duan, G. Merino, A. Rubio, *Phys. Rev. B* **2013**, *88*, 035432.
[22] Z.-X. Guo, S. Furuya, J.-I. Iwata, A. Oshiyama, *Phys. Rev. B* **2013**, *87*, 235435.
[23] Y. Yuan, R. Quhe, J. Zheng, Y. Wang, Z. Ni, J. Shi, J. Lu, *Phys. E* **2014**, *58*, 38.
[24] D. Tsoutsou, E. Xenogiannopoulou, E. Golias, P. Tsipas, A. Dimoulas, *Appl. Phys. Lett.* **2013**, *103*, 231604.
[25] S. Huang, W. Kang, L. Yang, *Appl. Phys. Lett.* **2013**, *102*, 133106.
[26] J. Avila, P. De Padova, S. Cho, I. Colambo, S. Lorcy, C. Quaresima, P. Vogt, A. Resta, G. Le Lay, M. C. Asensio, *J. Phys.: Condens. Matter* **2013**, *25*, 262001.
[27] A. Resta, T. Leoni, C. Barth, A. Ranguis, C. Becker, T. Bruhn, P. Vogt, G. Le Lay, *Sci. Rep.* **2013**, *3*, 2399.
[28] R. Arafune, C.-L. Lin, K. Kawahara, N. Tsukahara, E. Minamitani, Y. Kim, N. Takagi, M. Kawai, *Surf. Sci.* **2013**, *608*, 297.
[29] H. Enriquez, S. Vizzini, A. Kara, B. Lalmi, H. Oughaddou, *J. Phys.: Condens. Matter* **2012**, *24*, 314211.
[30] D. Kaltsas, L. Tsetseris, A. Dimoulas, *J. Phys.: Condens. Matter* **2012**, *24*, 442001.
[31] K. Schwarz, P. Blaha, G. Madsen, D. Kvasnicka, J. Luitz, *Wien2k: An Augmented Plane Wave + Local Orbitals Program for Calculating Crystal Properties,* Universität Wien, Austria **2001**.
[32] J. Perdew, K. Burke, M. Ernzerhof, *Phys. Rev. Lett.* **1996**, *77*, 3865.
[33] A. D. Becke, E. R. Johnson, *J. Chem. Phys.* **2006**, *124*, 221101.
[34] K. Momma, F. Izumi, *J. Appl. Crystallogr.* **2011**, *44*, 1272.
[35] E. Cinquanta, E. Scalise, D. Chiappe, C. Grazianetti, B. van den Broek, M. Houssa, M. Fanciulli, A. Molle, *J. Phys. Chem. C* **2013**, *117*, 16719.
[36] C.-L. Lin, R. Arafune, K. Kawahara, M. Kanno, N. Tsukahara, E. Minamitani, Y. Kim, M. Kawai, N. Takagi, *Phys. Rev. Lett.* **2013**, *110*, 076801.
[37] A. Moewes, E. Z. Kurmaev, J. S. Tse, M. Geshi, M. J. Ferguson, V. A. Trofimova, Y. M. Yarmoshenko, *Phys. Rev. B* **2002**, *65*, 153106.
[38] K. Schwarz, A. Neckel, J. Nordgren, *J. Phys. F: Met. Phys.* **1979**, *9*, 2509.
[39] P. De Padova, J. Avila, A. Resta, I. Razado-Colambo, C. Quaresima, C. Ottaviani, B. Olivieri, T. Bruhn, P. Vogt, M. C. Asensio, G. Le Lay, *J. Phys.: Condens. Matter* **2013**, *25*, 382202.
[40] P. De Padova, P. Vogt, A. Resta, J. Avila, I. Razado-Colambo, C. Quaresima, C. Ottaviani, B. Olivieri, T. Bruhn, T. Hirahara, T. Shirai, S. Hasegawa, M. C. Asensio, G. Le Lay, *Appl. Phys. Lett.* **2013**, *102*, 163106.
[41] P. Vogt, P. Capiod, M. Berthe, A. Resta, P. De Padova, T. Bruhn, G. Le Lay, B. Grandidier, *Appl. Phys. Lett.* **2014**, *104*, 021602.